17. Brune, J. and Singh, D., Continent-like crustal thickness beneath the Bay of Bengal sediments. *Bull. Seismol. Soc. Am.*, 1986, **76**, 191–203.
18. Wiens, D. A., Stein, S., Demets, C., Gordon, R. G. and Stein, C., Plate tectonic models for Indian Ocean intraplate deformation. *Tectonophysics*, 1996, **132**, 37–48.
19. Stein, S. and Okal, E. A., Seismicity and tectonic of the Ninetyeast Ridge area: Evidence for internal deformation of the Indian plate. *J. Geophys. Res.*, 1978, **83**, 2233–2245.
20. Subrahmanyam, C., Gireesh, R., Chand, S., Kamesh Raju, K. A. and Rao, D. G., Geophysical characteristics of the Ninetyeast Ridge – Andaman island arc/trench convergent zone. *Earth Planet. Sci. Lett.*, 2008, **266**, 29–45.
21. Socquet, A., Vigny, C., Chamot-Rooke, N., Simons, W., Rangin, C. and Ambrosius, B., India and Sunda plates motion and deformation along their boundary in Myanmar determined by GPS. *J. Geophys. Res.*, 2006, **111**, B05406; doi:10.1029/2005JB003877.
22. Havskov, J. and Ottemoller, L., Seis An earthquake analysis software. *Seismol. Res. Lett.*, 1999, **70**, 532–534.
23. Goldstein, P., Dodge, M. and Firpo, L. M., SAC availability for IRIS Community. *IRIS Newsl.*, 2005.
24. Pasyanos, M., Masters, T., Laske, G. and Ma, Z., LITHO1.0: an updated crust and lithospheric model of the Earth. *J. Geophys. Res.*, 2014; doi: 10.1002/2013JB010626.
25. Lienert, B. R. E. and Havskov, J., A computer program for locating earthquakes both locally and globally. *Seismol. Res. Lett.*, 1995, **66**, 26–36.
26. Lienert, B. R. E., Berg, E. and Frazer, L. N., Hypocenter: an earthquake location method using centered, scaled, and adaptively least squares. *Bull. Seismol. Soc. Am.*, 1986, **76**, 771–783.
27. Engdahl, E. R., Hilst, R. V. D. and Buland, R., Global teleseismic earthquake relocation with improved travel times and procedures for depth determination. *Bull. Seismol. Soc. Am.*, 1998, **88**, 722–743.
28. McCaffrey, R. and Abers, J., SYN3: a program for inversion of teleseismic body wave form on microcomputers, Technical Report AFGL-TR-0099, Air Force Geophysical Laboratory, Hanscomb Air Force Base, Massachusetts, 1998.
29. McCaffrey, R., Abers, G. and Zwick, P., Inversion of teleseismic body waves. International Association of Seismology and Physics of the Earth's Interior, 1991, **3**, 81–166.
30. Futterman, W., Dispersive body waves. *J. Geophys. Res.*, 1962, **67**, 5279–5291.
31. Gupta, S., Mohanty, W. K., Mandal, A. and Misra, S., Ancient terrane boundaries as probable seismic hazards: a case study from the northern boundary of the Eastern Ghats Belt India. *Geosci. Front.*, 2014, **5**, 17–24.
32. Wessel, P. and Smith, W. H. F., New, improved version of the generic mapping tools released. *EOS Trans. AGU*, 1998, **79**, 579.
33. Mahesh, *et al*., Rigid Indian plate constraints from GPS measurements. *Gondwana Res.*, 2012, **22**, 1068–1072.
34. Sandwell, D. T. and Smith, W. H. F., Global marine gravity from retracked geosat and ers-1 altimetry: ridge segmentation versus spreading rate. *J. Geophys. Res.*, 2009, **114**, B01411.

ACKNOWLEDGEMENTS. We thank Incorporated Research Institutions for Seismology (IRIS), Data Management Center (DMC), Washington for providing earthquake waveform data. Figures were prepared using Generic Mapping Tools[32].

Received 28 June 2014; revised accepted 4 March 2015

# The admissible tsunamigenic source region of 24 September 2013 land-based earthquake – application of backward ray tracing technique

**Ch. Patanjali Kumar*, B. Ajay Kumar, E. Uma Devi, R. S. Mahendra, M. V. Sunanda, M. Pradeep Kumar, J. Padmanabham, S. Dipankar and T. Srinivasa Kumar**

Indian National Centre for Ocean Information Services (INCOIS), Hyderabad 500 090, India

**A minor tsunami of about 50 cm was generated along the coast of Qurayat near Makran subduction zone in the Arabian Sea due to the 24 September 2013 Pakistan earthquake of magnitude 7.6 $M_w$(mB), although its source was ~200 km far inland of the Makran trench. The real-time sea-level observation network in the Arabian Sea recorded minor tsunami arrivals. In an attempt to explain the mechanism of this unusual tsunami, we use backward ray tracing technique to map the admissible region of tsunamigenic source. Basically, in this technique the ray equations are integrated starting from the specific locations of tsunami observations, in all possible directions. The known travel time of the initial waves to the respective tide gauges and tsunami buoys is used in this method. Backward wave front is constructed by joining all end-points of the rays from each of the locations. The region where the envelope of all backward wave fronts converges is considered as the source of the tsunami, which is ~470 km from the earthquake epicentre with the location at 24.8 N and 61.5 E. The admissible region identified is an undersea section between Chabahar and Gwadar, where a mud island had appeared subsequent to this earthquake. Convergence of the tsunami source zone and location of the mud island suggest that the sudden uplift must have caused the tsunami.**

**Keywords:** Backward ray tracing, earthquake, tsunami, subduction zone.

ON 24 September 2013 at 11:29 UTC, an earthquake of magnitude 7.6 $M_w$(mB) occurred ~200 km away from the Makran coast of Pakistan. It was located ~280 km NW of Karachi, 26.99 N and 65.52 E (location obtained by ITEWS auto-location software) with a hypocentral depth of 10 km (Figure 1). This earthquake triggered a tsunami that was recorded by various sea-level tide gauges along the coastal regions of the Arabian Sea and tsunami buoys in the Arabian Sea. Based on the global experiences, it is known that tsunamis are usually generated by undersea shallow-focus earthquakes. Co-seismic or delayed tsunami generation due to submarine landslides or slumps is

*For correspondence. (e-mail: patanjali@incois.gov.in)

another cause of tsunamis, as demonstrated by the classic example of the 1929 Great Banks earthquakes[1]. The Makran subduction zone is believed to have triggered delayed tsunamis, possibly by submarine slides during the 1945 earthquake sourced close to the trench[2]. While these earthquakes were sourced close to the trench, the source of the 2013 earthquake was ~200 km inland and the tsunami that followed is unusual. Such events exemplify the underestimated tsunami hazard and call for better understanding of the tsunamigenic potential of near-coast bathymetric features, accretionary complex off Makran coast[3]. A clearer understanding of these features and their potential role in tsunami generation is important while designing tsunami early warning systems. Here we briefly summarize the current status of the Indian Tsunami Early Warning System (ITEWS) and the seismotectonic background of the earthquake source and argue that the tsunami was triggered by the mud volcano.

The ITEWS, which is the first tsunami early warning system in the Indian Ocean[4], has established a real-time sea-level observation network (tsunami buoys and tide gauges) in the Indian Ocean to detect tsunamigenic events from the Andaman–Sumatra subduction arc and Makran subduction zone. Tsunami buoys (consisting of bottom pressure recorder and surface buoy) are deployed close to the tsunamigenic source regions in the Bay of Bengal and Arabian Sea. The deployment and maintenance of these buoys are being done in collaboration with the National Institute of Ocean Technology (NIOT), Chennai and M/s SAIC, USA. The tsunami buoys are capable of detecting minor water-level changes of even 1 cm at water depths up to 6 km. The data are transmitted in real-time through satellite communication for processing and interpretation. Apart from tsunami buoys, state-

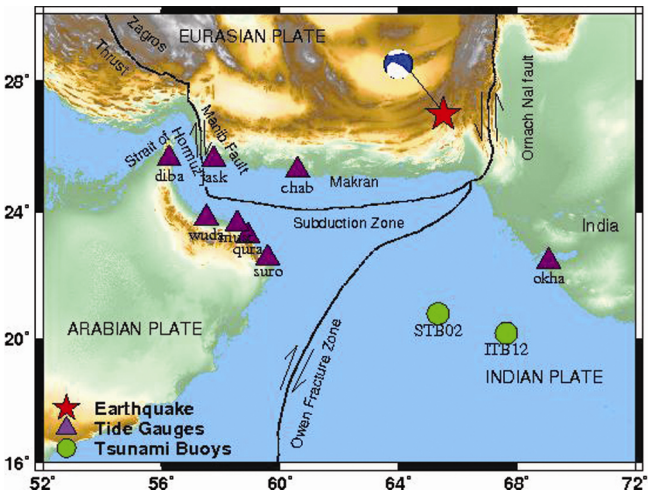


**Figure 1.** Map of the northwestern Indian Ocean region with major tectonic features with the epicentre of the 24 September 2014 Pakistan earthquake indicated by a red star along with its focal mechanism solution (Global CMT Catalog). The sea-level observation network which recorded the tsunami waves also plotted (dark pink triangles represent tide gauge and green circles are the Indian tsunami buoy).

of-the-art tide gauges are also installed at strategic locations along the Indian coast and islands to monitor the progress of tsunami waves as well as for validation of the tsunami model results. Three types of tide gauge sensors: pressure, radar and shaft encoder are installed at each location. The installation and maintenance of these tide gauges are being done in collaboration with Survey of India (SoI), Dehradun and M/s SGS Weather and Environmental Systems, New Delhi. The data are transmitted in real time through different modes of communication like INSAT, GPRS, VSAT simultaneously for processing and interpretation.

The 24 September 2013, 7.6 $M_w$(mB) earthquake in south-central Pakistan, referred in the literature as Balochistan earthquake, is believed to have nucleated on the near N–S-oriented, ~1200 km long Chaman fault with a left-lateral strike–slip motion[5]. The initial solution suggests its source at shallow crustal depths, which has been further modelled by Avouac *et al.*[5] as less than 15 km. The earthquake occurred within the transition zone between northward subduction of the Arabia plate beneath the Eurasia plate and northward collision of the India plate with the Eurasia plate[6]. The strike–slip solution with a thrust component seems to be consistent with the northward motion of the western side of India with respect to Eurasia at 3 cm/yr, which is accommodated across the Chaman fault system[7].

The ~1000 km-long Makran subduction zone has resulted from the convergence between the Eurasian and Arabian plates[2]. The convergence has led to the development of one of the thickest accretionary wedges, with an estimated thickness[8,9] of ~7 km. Exposure of a sedimentary wedge about 500 km wide has been reported[10,11] from the onshore Pakistan and Iran. The offshore Makran accretionary complex with five major structural provinces and elements[12], consists of largely unconsolidated sediments. The offshore Makran accretionary prism is located at depth of 750–3000 m, but it has been reported that there is no bathymetric trench seaward of the deformation front (at ~3000 m) depth, due to the large sediment influx[13]. Smith *et al.*[13] also quote sources that report the common occurrence of mud volcanoes onshore, which they believe to be associated with E–W-trending fault zones.

Byrne *et al.*[14] proposed that a large quantity of unconsolidated sediment does not necessarily indicate a low potential for great thrust earthquakes. However, in regions of large sediment thickness, it has been suggested that the accretionary prism provides large volumes of material with weak mechanical properties, where rupture propagation is slow. Examples of tsunami triggered by the transfer of stresses to the accretionary wedge are discussed in the literature[15].

A real-time network of sea-level stations is a crucial requirement for the tsunami warning system to confirm whether the undersea earthquake has actually triggered a

tsunami or not. It is essential to measure the changes in water level in real-time with high accuracy to upgrade or downgrade tsunami advisories in real time[16]. ITEWS, at Indian National Centre for Ocean Information Services (INCOIS) has configured a software to receive, quality control, archive, process and analyse the real-time data from the tsunami buoys and tide gauge network as well as for alert generation and automatic notification of any significant water-level changes/communication delays. The de-tide (predicted data subtracted from observed) data have been computed using SLPR2 software[17] for all national sea-level stations to distinguish tsunami waves from normal tidal waves. Real-time observations of sea level can then be used to 'invert' for slip parameter and update the forecast.

Two tsunami buoys, STB02 (20.80N, 65.34E) and ITB12 (20.18N, 67.65E), were deployed in the Arabian Sea to detect and monitor the tsunamis originating from Makran subduction zone, as part of one of its tsunami warning system components[18]. The tsunami buoys STB02 and ITB12 got triggered by seismic Rayleigh waves at 1130 and 1131 UTC simultaneously and started reporting in 'tsunami mode' to the Tsunami Early Warning Centre at INCOIS. A tsunami wave of 1 cm was observed at 1225 UTC in STB02 and 1.1 cm in ITB12 at 1240 UTC. The location of the sea-level stations which recorded the tsunami wave is given in Figure 1.

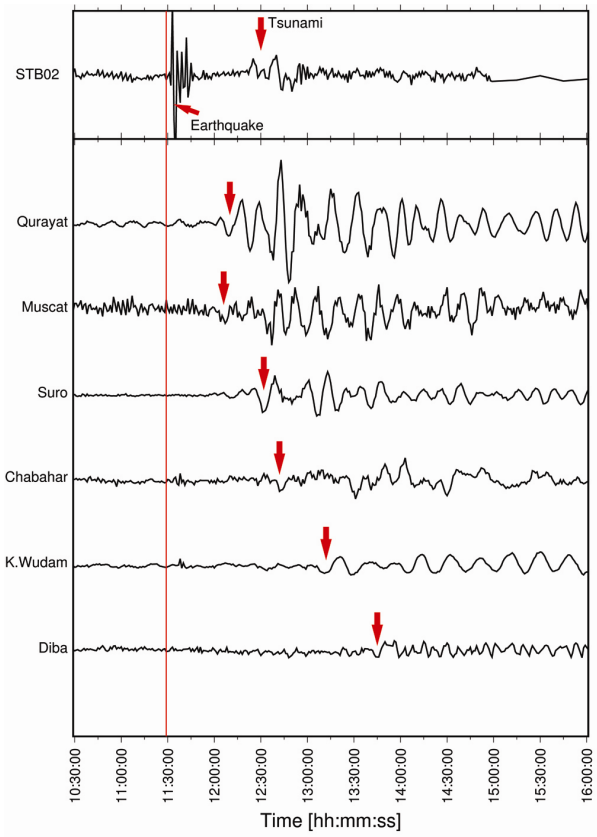


**Figure 2.** Minor tsunami wave observations at different sea-level stations in the Arabian Sea on 24 September 2013. (Red line indicates the earthquake origin time and arrows indicate the tsunami wave arrival time.)

The arrival of the first tsunami wave to Qurayat (Oman), Muscut (Oman) and Suro (Oman) tide gauges was at 1205, 1206, 1208 UTC respectively, and tsunami waves of 57, 22 and 20 cm respectively, were observed. Chabahar (Iran) tide gauge also observed 19 cm wave at 1240 UTC (Figure 2).

The ray diagram technique also referred as refraction diagram is one of the many techniques used to model tsunami waves. The technique is fast when compared with other numerical modelling techniques where accuracy is sacrificed for computational speed. The technique was initially proposed by Miyabe[19] to investigate the Saniruku tsunami of 1933, and also used by Satake[20] to analyse bathymetry effects on tsunami propagation.

The ray diagram technique models the propagation of the 'leading edge' of the tsunami waves and can be used to compute the travel times of the waves from the source to any desired location. As this approach does not compute the amplitudes of the waves, all amplitude information is sacrificed along with accuracy. The inverse problem of the above-mentioned approach (mapping source from travel times), popularly known as backward ray tracing technique, can be used to easily map the source region[21,22].

The ray equations are derived from the linearized shallow-water equations using the eikonal approximation and smoothening of the bathymetry is required to apply the same to tsunami waves.

The tsunami waves can be described by the nonlinear shallow-water equations on a spinning sphere with nonlinearities, the curvature of the earth and Coriolos force.

The set of points in a wave with the same phase are called wavefronts, which define the wave propagation in time. The rays can be represented as the trajectory of a corpuscule normal to the wavefront travelling with the speed of the wavefront. For a small area of interest, the nonliner shallow-water wave equations of the tsunami can be approximated by neglecting the effects of curvature of the earth and Coriolos force with linearized equations. The solutions of approximated, linearized equations are the linear combination of waves with specific frequencies, those which satisfy Helmholtz equation. The ray equations on the plane can be written as

$$\frac{\mathrm{d}x_{\mathrm{R}}}{\mathrm{d}t} = c\cos\chi,$$

$$\frac{\mathrm{d}y_{\mathrm{R}}}{\mathrm{d}t} = c\sin\chi,$$

$$\frac{\mathrm{d}\chi}{\mathrm{d}t} = -\sin\chi\frac{\partial c}{\partial x} + \cos\chi\frac{\partial c}{\partial y}.$$

It is clear from the ray equations that the rays are independent of the frequency of the wave and only depend on bathymetry. Thus in the case of tsunamis, the rays can be assumed as wave packets containing a range of frequencies, which are dispersion-less for a flat bathymetry. The ray theory can be applied to tsunamis only if bathymetry is smoothened, as the above ray equations are derived for such wavelengths being much smaller than the length scale at which the bathymetry varies. Further, the ray equations can be integrated starting from the specific locations of tsunami observations, in all possible directions, for the known tsunami observed travel time of initial waves. Then the backward wavefront can be constructed by joining all the end-points of the rays from each location. And the envelope of all backward wavefronts defines the required curve that is a boundary for the source region of interest[21].

The bathymetry is smoothened by considering the wavelengths of interest in order to apply the ray theory in this study. It is done by replacing the speed at any point by average of the speeds of all points in a box of length approximate to wavelength around it[23], i.e. for a given bathymetry on a grid point, the corresponding wave speeds computed to define the smoothened bathymetry by choosing the physical length of the box approximate to wavelength. For near-shore points, all land points in the box are removed[21].

In this case study, the ray diagrams are constructed starting from each location of sea-level gauge, in all possible directions, for the respective observed travel time of initial tsunami waves. The initial tsunami wave arrival at each sea-level gauge is noted and listed in Table 1. Then the backward wavefront is constructed by joining all the end-points of the rays from each location. Finally, the envelope of all backward wavefronts from every sea-level gauge defines the required curve that is the boundary for the source region of interest.

**Table 1.** Water-level variations recorded at various sea-level observation stations located in and along the Arabian Sea

| Station (country) | Latitude (°N) | Longitude (°E) | Observed time of first arrival (UTC) | Observed maximum wave height (cm) |
|---|---|---|---|---|
| Qurayat (Oman) | 23.26 | 58.92 | 1205 | 57 |
| Muscut (Oman) | 23.633 | 58.566 | 1206 | 22 |
| Suro (Oman) | 22.57 | 59.59 | 1208 | 20 |
| STB02 (India) | 20.80 | 65.34 | 1225 | 1.0 |
| Chabahar (Iran) | 25.29 | 60.60 | 1240 | 19 |
| ITB12 (India) | 20.18 | 67.65 | 1255 | 1.1 |
| Khawr Wudam (Oman) | 23.82 | 57.52 | 1314 | 11 |
| Diba (Oman) | 25.64 | 56.26 | 1345 | 08 |
| Jask (Iran) | 25.63 | 57.77 | 1412 | 06 |
| Okha (India) | 22.46 | 69.08 | 1712 | 02 |

Though the epicentre was located inland approximately 200 km away from near coast, the tsunamigenic source region – the admissible region mapped by the backward ray tracing technique was between Chabahar and Gwadar as indicated in Figure 3. This was the same location where the mud island had appeared as a consequence of the strike–slip faulting of this earthquake. The sudden uplift of the mud island might have caused the tsunami generation, which was clearly mapped by the backward ray tracing technique in this case study.

Thus the ITEWS has the responsibility to provide timely tsunami advisories not only to India as the National Tsunami Warning Centre, but also to Indian Ocean rim countries in its area of responsibility (AOR) as one of the Regional Tsunami Advisory Service Providers for the Indian Ocean. The performance of Indian Tsunami Early Warning Centre (ITEWC) is 100% for detection of earthquakes and monitoring tsunamis in the Indian Ocean[24] and the same was proved in case of the 11 April 2012 Sumatra earthquake[16]. The tsunami triggered as the consequence effects of inland earthquake of magnitude 7.6 $M_w$(mB) on 24 September 2013 was recorded by Indian tsunami buoys (STB02 and ITB12) and tide gauges as well as Indian Ocean sea-level observation network. This was the first case in ITEWC where a

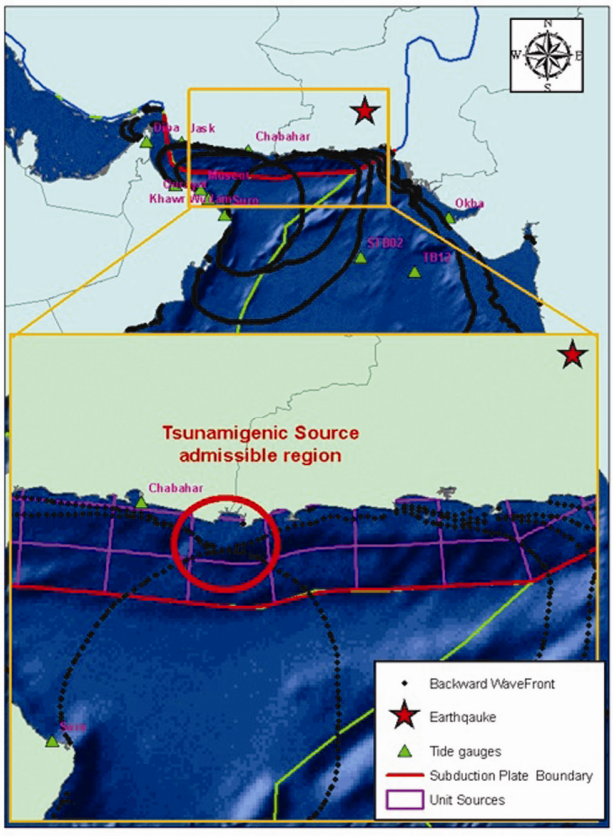


**Figure 3.** Admissible tsunamigenic region obtained by backward ray tracing technique marked as red circle.

tsunami got triggered by land-based earthquake of magnitude 7.6 $M_w$(mB). The simple backward ray tracing method was applied for gross delimitation of the tsunami source region utilizing the tsunami arrival times recorded by sea-level observation networks. There is a limitation to this approach as it does not take advantage of the information of wave amplitude and shape, thus providing little information about the tsunami source. Further detailed study and analysis of all available bathymetric, seismic and seismological, geophysical and geodetic data are required to exactly constrain the tsunamigenic source further. The wave inversion method using Greens function technique to invert 'equivalent' co-seismic slip for preset unit sources will be used in a future study.

The backward ray tracing technique which is considered the most effective way to determine the tsunamigenic source area and mapping of the admissible region, is well proved in this case and it provides the first-hand information about the admissible region – tsunamigenic source that generated the tsunami as the consequence effects of inland earthquake. In this case, admissible region was mapped as an undersea area between Chabahar and Gwadar regions, which is ~470 km from the earthquake epicentre with locations at 24.8 N and 61.5 E. This was the same location where the mud island had appeared as a consequence of the strike–slip faulting of this earthquake[25]. The sudden uplift of mud island or submarine slumping might have caused the tsunami generation, which could be clearly mapped by the backward ray tracing technique as admissible tsunamigenic source. This study reiterates the need to have better assessment of the tsunamigenic potential of accretionary prisms, which themselves may not generate an earthquake, but their co-seimic deformation can in turn trigger tsunamis. This aspect of tsunami mechanism cannot be ignored, especially for locations such as the Makran which hosts one of the thickest accretionary prisms.


1. Hasegawa, H. S. and Kanamori, H., Source mechanism of the magnitude 7.2 Grand Banks earthquake of 18 November 1929: double-couple or submarine landslide? *Bull. Seismol. Soc. Am.*, 1987, **77**, 1984–2004.
2. Rajendran, C. P., Rajendran, K., Shah-Hosseini, M., Abdolmajid, N. B., Nautiyal, C. M. and Ronia, A., The hazard potential of the western segment of the Makran subduction zone, northern Arabian Sea. *Nat. Hazards*, 2013, **65**, 219–239; doi:10.1007/s11069-012-0355-6.
3. Jolivet, R. *et al.*, The 2013 $M_w$ 7.7 Balochistan earthquake: seismic potential of an accretionary wedge. *Bull. Seismol. Soc. Am.*, 2014, **104**(2), 1020–1030.
4. Nayak, S. and Srinivasa Kumar, T., The first tsunami warning centre in the Indian Ocean. In *Risk Wise*, Tudor Rose Publishers, UK, 2008, pp. 175–177.
5. Avouac, J. P. *et al.*, The 2013, $M_w$ 7.7 Balochistan earthquake, energetic strike–slip reactivation of a thrust fault. *Earth Planet. Sci. Lett.*, 2014, **391**, 128–134.
6. USGS, 2013; http://earthquake.usgs.gov/earthquakes/eqarchives/poster/2013/20130924.php
7. Szeliga, W., Bilham, R., Kakar, D. M. and Lodi, S. H., Interseismic strain accumulation along the western boundary of the Indian subcontinent. *J. Geophys. Res., Solid Earth*, 2012, **117**, B08404; doi:10.1029/2011JB008822.
8. Kopp, C., Fruehn, J., Flueh, E. R., Reichert, C., Kukowski, N., Bialas, J. and Klaeschen, D., Structure of the Makran subduction zone from wide-angle and reflection seismic data. *Tectonophysics*, 2000, **329**, 171–191.
9. Kukowski, N., Schillhom, T., Flueh, E. R. and Huhn, K., A newly identified strike slip plate boundary in the north-east Arabian Sea. *Geology*, 2000, **28**, 355–358.
10. Schluter, Prexl, A., Gaediche, Ch., Roeser, H., Reichert, Ch., Meyer, H. and Daniels, C. V., The Makran accretionary wedge: sediment thickness and ages and the origin of mud volcanoes. *Mar. Geol.*, 2002, **185**, 219–232.
11. Kukowski, N., Schillhom, T., Huhn, K., Rad, U. V., Husen, S. and Flueh, E. R., Morphotectonics and mechanics of the central Makran accretionary wedge off Pakistan. *Mar. Geol.*, 2001, **173**, 1–19.
12. Mokhtari, M., Fard, I. A. and Hessami, K., Structural elements of the Makran region, Oman sea and their potential relevance to tsunamigenisis. *Nat. Hazards*, 2008, **47**, 185–199; doi:10.1007/s11069-007-9208-0.
13. Smith, G., McNeill, L., Henstock, T. J. and Bull, J., The structure and fault activity of the Makran accretionary prism. *J. Geophys. Res.*, 2012, **117**, B07407; doi:10.1029/2012JB009312.
14. Byrne, D. E., Sykes, L. R. and Davis, D. M., Great thrust earthquakes and aseismic slip along the plate boundary of the Makran subduction zone. *J. Geophys. Res.*, 1992, **97**, 449–478.
15. Okal, E. A. and Newmann, A. V., Tsunami earthquakes: the quest for a regional signal. *Phys. Earth Planet. Inter.*, 2001, **124**, 45–70.
16. Srinivasa Kumar, T. *et al.*, Successful monitoring of the 11 April 2012 tsunami off the coast of Sumatra by Indian Tsunami Early Warning Center. *Curr. Sci.*, 2012, **102**(11), 1519–1526.
17. Caldwell, P., Sea level data processing on IBM-PC compatible computers, version 3.0, JIMAR Contribution No 98-319, University of Hawaii, Manoa, 1998.
18. Nayak, S. and Srinivasa Kumar, T., Addressing the risk of tsunami in the Indian Ocean. *J. South Asia Disaster Stud.*, 2008, **1**(1), 45–57.
19. Miyabe, N., An investigation of the Sanriku tsunami based on Mareogram data. *Bull. Earthquake Res. Inst. Tokyo Univ. Suppl.*, 1934, **1**, 112–126.
20. Satake, K., Effects of bathymetry on tsunami propagation: application of ray tracing to tsunami. *Pageoph*, 2001, **126**(1), 27–36.
21. Shankar, R., Retracing the tsunami waves. In *Tsunami and Nonlinear Waves* (ed. Kundu, A.), 2007, pp. 265–272.
22. Neetu, S. *et al.*, Comment on 'The Great Sumatra–Andman Earthquake of 26 December 2004'. *Science*, 2005, **310**, 1431.
23. Sindhu, B., Suresh, I., Unnikrishnan, A. S., Bhatkar, N. V., Neetu, S. and Michael, G. S., Improved bathymetric datasets for the shallow water regions in the Indian Ocean. *J. Earth Syst. Sci.*, 2007, **116**(3), 261–274.
24. Srinivasa Kumar, T. *et al.*, Performance of the tsunami forecast system for the Indian Ocean. *Curr. Sci.*, 2012, **102**(1), 110–114.
25. BBC, Pakistan quake island off Gwadar emits flammable gas; http://www.bbc.com/news/world-asia-24272552


ACKNOWLEDGEMENTS. We thank the Ministry of Earth Sciences (MoES), New Delhi for support and encouragement; and our colleagues at SOI, NIOT, INCOIS and MoES for support in developing and operating this state-of-the-art system. We also thank IOC (IODE) for sea-level data facility of tide gauges deployed and operated by other countries in the Indian Ocean. Few figures have been generated using GMT freeware developed by Paul Wessel and Walter H. F. Smith. This is INCOIS publication 217.

Received 19 June 2014; revised accepted 2 March 2015